Direct observation of mammalian cell growth and size regulation

Sungmin Son[1,2], Amit Tzur[3,6], Yaochung Weng[1,4], Paul Jorgensen[3], Jisoo Kim[2], Marc W Kirschner[3] & Scott R Manalis[1,2,4,5]

We introduce a microfluidic system for simultaneously measuring single-cell mass and cell cycle progression over multiple generations. We use this system to obtain over 1,000 h of growth data from mouse lymphoblast and pro–B-cell lymphoid cell lines. Cell lineage analysis revealed a decrease in the growth rate variability at the G1-S phase transition, which suggests the presence of a growth rate threshold for maintaining size homeostasis.

The lack of consensus on how mammalian cells grow across generations[1–7] may largely stem from technical limitations. Almost all prior studies of size homeostasis have monitored populations of cells. In a typical experiment, the cell cycle of a population of cells would be synchronized and the average cell size monitored over time as the synchronized cells grew and eventually divided. Such experiments are limited not only by the poor resolution afforded by cell cycle synchronization and the unavoidable dispersion that follows, but also by artifacts produced by the synchronization methods themselves. Techniques for synchronization typically block nuclear division but not cell growth and inevitably result in oversized cells[4,5]. In the most comprehensive single-cell study yet to examine the inter-relationship of cell growth and the cell cycle, single yeast cells were studied microscopically using a fluorescent reporter protein as a proxy for cell mass[8]. By correlating cell mass to specific cell cycle events, a cell size threshold for cell cycle entry was observed. Although protein content may be the dominant component within a cell, the use of a fluorescent reporter protein does not guarantee a precise readout of a cell's biomass. In contrast, various forms of microscopy for measuring cell dry mass have been applied to cell growth, but they have generally suffered from limited precision[9].

To overcome the technical problems that have limited the study of cell growth, we recently developed a direct approach for dynamically monitoring the mass of individual growing cells. We have demonstrated that this method, which uses a suspended microchannel resonator (SMR) mass sensor, has the potential to weigh animal cells with a precision near 0.01% (ref. 10). The SMR measures the buoyant mass of objects that pass through it. When an object that is denser than the surrounding fluid passes through the device, the net increase in mass (that is, the buoyant mass of the object) lowers the resonant frequency. By continually measuring buoyant mass as the cell travels back and forth through the sensor, the growth of individual bacteria, yeast and mammalian cells has been observed[11]. However, the resulting continuous shear stress limited the growth duration to less than 1 h, the method was not configured to observe cell cycle progression, and uncertainty introduced by the fluidic control system effectively limited the buoyant mass precision to ~1%.

Here we describe three technological advancements for the SMR that enable precise measurement of cell growth and cell cycle progression. First, an individual cell and its progeny can be weighed over many generations. Storing the cell in a large bypass reservoir and only occasionally passing it through the SMR ensures that the cell experiences only limited exposure to shear forces (**Fig. 1a**, **Supplementary Video 1** and Online Methods). The interdivision time for single L1210 mouse lymphoblast cells in this new apparatus is similar to its doubling time in culture, suggesting that cell growth is unperturbed (**Supplementary Fig. 1**). Second, we have used a unique form of hydrodynamic focusing to confine the flow path of the cell as it travels through the SMR (**Supplementary Fig. 2**). Without such focusing, the cell can wander in a direction orthogonal to the flow stream, which creates position-dependent error. Hydrodynamic focusing enables the cell's buoyant mass and growth rate to be measured with precisions near 0.05% and 3%, respectively, which represent a tenfold improvement over prior work[11]. Third, we have integrated a microscope with the SMR so that a cell can be observed while it is stored within the bypass channel (**Fig. 1a**). This enables monitoring of cell cycle events using fluorescent ubiquitination-based cell cycle indicators (FUCCI)[12]. In the experiments reported here, L1210 mouse lymphoblast cells stably express fluorescently tagged proteins that are only present during early to late G1 phase of the cell cycle (mKO2-Cdt1, red fluorescence) or during S, G2 and early M phases (geminin-mAG, green fluorescence). Fluorescent signals are monitored concurrently with cell buoyant mass over multiple generations (**Fig. 1b**), which allows size and changes in growth properties to be linked to cell cycle position.

Because the growth of single cells has never been measured before with such precision, we could identify previously

[1]Koch Institute for Integrative Cancer Research, Massachusetts Institute of Technology (MIT), Cambridge, Massachusetts, USA. [2]Department of Mechanical Engineering, MIT, Cambridge, Massachusetts, USA. [3]Department of Systems Biology, Harvard Medical School, Boston, Massachusetts, USA. [4]Computational and Systems Biology Initiative, MIT, Cambridge, Massachusetts, USA. [5]Department of Biological Engineering, MIT, Cambridge, Massachusetts, USA. [6]Present address: The Mina and Everard Goodman Faculty of Life Sciences and Advanced Materials and Nanotechnology Institute, Bar-Ilan University, Ramat-Gan, Israel. Correspondence should be addressed to S.R.M. (scottm@media.mit.edu).

RECEIVED 4 MAY; ACCEPTED 10 JULY; PUBLISHED ONLINE 5 AUGUST 2012; DOI:10.1038/NMETH.2133

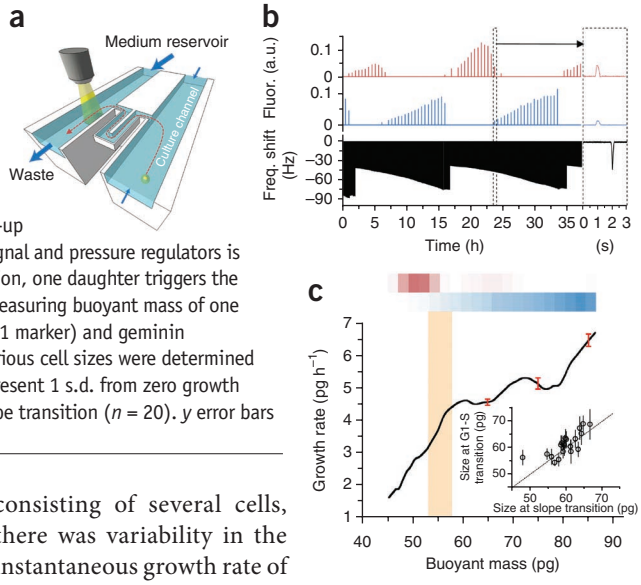

Figure 1 | Measurement of single-cell growth and cell cycle progression. (**a**) Pressure-driven flow (blue arrows) moves a cell between bypass channels and provides fresh medium between measurements. The cell is weighed as it passes through the SMR (red path). Fluorescent signals are measured when the cell passes through the optical window in the bypass reservoir (yellow). (**b**) Mass (black, measured every 30 s) and fluorescent signals from the cell cycle reporters (blue, Cdt1 and red, geminin; measured every 30 min) were acquired from an L1210 mouse lymphoblast cell over four generations (fluor., fluorescence in arbitrary units (a.u.); freq., frequency). The dashed box to the right of the arrow shows a close-up of signals from one transit through the SMR. Automated feedback between the mass signal and pressure regulators is used to transport the cell back and forth between the bypass channels. Following division, one daughter triggers the feedback, and the other is swept away. (**c**) Growth rate versus cell mass, obtained by measuring buoyant mass of one cell from the newborn stage through division. Color bar indicates relative Cdt1 (red, G1 marker) and geminin (blue, S/G2/M marker) levels. Yellow indicates the G1-to-S transition. Error bars at various cell sizes were determined by measuring the growth rate of a fixed (nongrowing) cell over a 12-h period and represent 1 s.d. from zero growth rate. Inset: correlation between the size at G1-S transition and size at the growth slope transition ($n = 20$). *y* error bars indicate the mass change between the maximum and following minimum Cdt1 levels.

undescribed aspects of the growth trajectory. Most striking is the transition in growth rate that occurred midway through the cell cycle. During the first several hours after cytokinesis, there was a rapid increase in growth rate followed by a period in which the growth rate increased more slowly (**Fig. 1c**), a behavior consistent with the prior population measurements on these cells[13]. Out of 122 cells measured, 50% showed a transition with a distinct change in growth rate, 20% showed a less distinct change in growth rate and the remainder showed erratic growth trajectories (**Supplementary Fig. 3**). We wondered if the growth rate transition might coincide with the transition of cells out of G1 phase—which is thought to be devoted largely to growth—and into S-phase, where DNA synthesis occurs. The FUCCI signals were measured over the complete cell cycle in 40 cells, of which 20 showed an obvious growth rate transition. There was a strong correlation between the growth rate transition and entry into S phase (**Fig. 1c**).

A unique benefit of single-cell growth trajectories is the ability to register cell-to-cell variability (**Fig. 2**). Within each lineage consisting of several cells, there was variability in the instantaneous growth rate of newborn cells that typically ranged from 2 to 4 pg h^{-1}, and these rates were independent of size (**Fig. 2a**). For a given lineage of cells, the variability in growth rate decreased as cells progressed through G1 and began to increase after the G1-S phase transition. The cell size at this transition point varied among different sets of lineages (**Supplementary Fig. 4**). Newborn cells closely related in lineage had different initial growth rates, yet they entered S phase with similar growth rates, an observation suggesting that there is a threshold in growth rate that gates the G1-to-S phase transition. Even among independent lineages, the coefficient of variance of growth rate at birth decreased to about 60% at the G1-S phase transition (**Fig. 2e**). We also observed a reduction in size variation between birth and the G1-S transition, although to a much smaller extent (1.7%). Furthermore, the growth rate–per–mass trajectories (**Fig. 2a** and **Supplementary Fig. 4**) saturated upon cell entry into S phase.

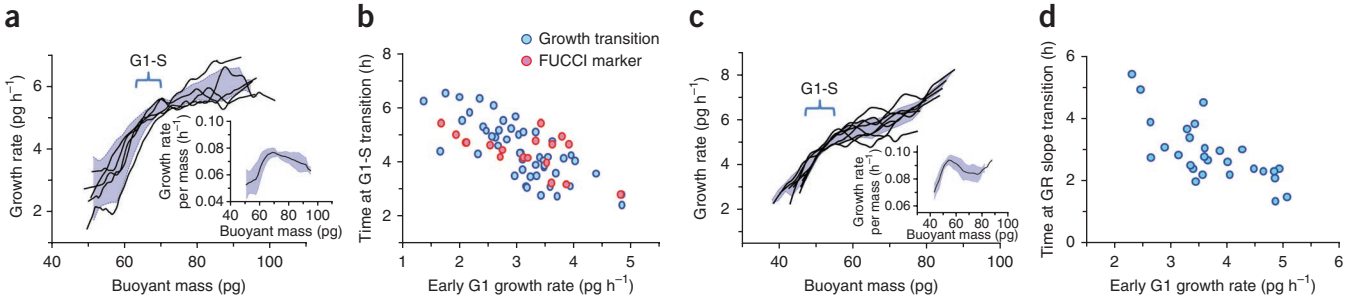

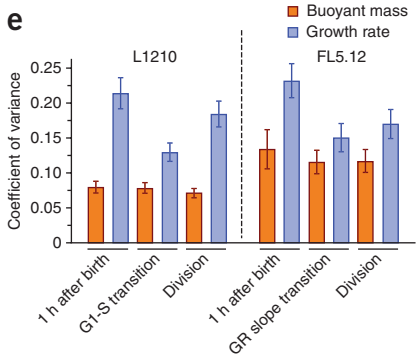

Figure 2 | Evidence for a growth rate threshold. (**a**) Single-cell growth rate trajectories (black lines) for a lineage of five L1210 cells. Blue area defines five times the coefficient of variance. Inset: mean (black line) and s.d. (blue area) of growth rate per unit mass from the lineage. (**b**) Time at G1-S phase transition versus early G1 growth rate (averaged between the first and third hour of growth following division) for L1210 cells. Blue and red circles signify G1-S transition defined by growth transition ($n = 49$, Pearson's correlation coefficient = –0.75) and by FUCCI ($n = 18$, Pearson's correlation coefficient = –0.60), respectively. (**c**) Single-cell growth rate trajectories (black lines) for a lineage of eight FL5.12 cells. Blue area defines five times the coefficient of variance. Inset depicts growth rate per unit mass as in **a**. (**d**) Time at G1-S phase transition versus early G1 growth rate (GR) for FL5.12 cells. G1-S transition is defined by calculating the growth transition point ($n = 28$, Pearson's correlation coefficient = –0.72). (**e**) Coefficient of variance (CV) for buoyant mass and growth rate at various points in the cell cycle. $n = 49$ for L1210; $n = 28$ for FL5.12. Error bars represent 1 s.d. of the CV from bootstrapping 1,000 times.

The rapid increase in growth rate per mass in G1 indicates that the growth rate is not simply proportional to cell mass and suggests that there may be unique regulation mechanisms established during the G1 phase of the cell cycle.

Further support for a growth rate threshold for entry into S phase comes from the strong negative correlation we observed between the duration of G1 and the growth rate in early G1 (**Fig. 2b**). Because all cells increase their growth rate in G1, slow-growing newborn cells may achieve the growth rate threshold by spending more time in G1. This trend became even more pronounced as we decreased the growth rate of cells by limiting nutrients (**Supplementary Fig. 5**). Furthermore, in contrast to the results of previous experiments with yeast in which small newborns tended to exhibit a prolonged G1 phase[14], we found that neither the duration of G1 nor the interdivision time correlated with newborn cell size (**Supplementary Fig. 6**). This, together with the findings shown in **Figure 2a**, suggests that deterministic growth regulation[15] can be based on a critical growth rate rather than a critical size.

To determine whether a growth rate threshold at the G1-S transition occurs in other types of cells, we measured growth trajectories of the FL5.12 pro–B-cell lymphoid cell line. **Supplementary Figure 7** shows an ~110-h continuous buoyant mass measurement of 12 generations of cells from the same lineage of FL5.12 and an analogous measurement for L1210 cells for comparison. Similarly to what we observed for L1210 cells, the variability in growth rate for FL5.12 cells decreased as cells progressed through G1 and then began to increase following the G1-S transition (**Fig. 2c**). Also consistent with our results using L1210 cells, there was a strong negative correlation between the G1 duration and growth rate in early G1 (**Fig. 2d**). Unlike L1210 cells, which showed no correlation between the duration of G1 or the interdivision time and newborn cell size, FL5.12 cells showed measurable but weak correlations (**Supplementary Fig. 6**).

Cell growth and cell size are known to adapt to external conditions[2]. To explore this in more detail, we grew L1210 cells in limiting isoleucine. Under these conditions, the growth rate was reduced and the duration of the G1 phase and interdivision time increased by 1.6-fold (**Supplementary Fig. 8a**). Despite this increase, the size range at both the G1-S phase transition and at cytokinesis remained virtually the same as cells in normal medium (**Supplementary Figs. 8b** and **9**). Furthermore, the presence of a strong negative correlation between the initial growth rate and the length of G1 (**Supplementary Fig. 5**) and a reduction in the variability of the growth rate at the G1-S phase transition (**Supplementary Fig. 10**) suggests that a growth rate threshold was still present.

Measurement of individual growth trajectories with a precision sufficient to register cell-to-cell variability reveals that growth and the cell cycle are tightly coupled in more complex ways than previously imagined. First, contrary to earlier notions that growth is either constant or simply a function of cell mass, there is a demonstrable, distinct change in growth rate at the G1-S transition, suggesting that growth and cell cycle are closely linked. Second, cells grown in nutrient-poor media have the ability to maintain their size at the G1-S transition and at cytokinesis by slowing cell cycle progression in proportion to their reduction in growth rate. Finally, the capacity of the SMR method to examine the trajectories of individual cells is what allowed us to conclude that the G1-S transition is not gated by a critical size threshold. Instead, the drop in growth rate variability suggests that the G1-S transition responds to a critical growth rate. Such a model could not be obtained without knowing the precise growth trajectories of individual cells. The critical role of a growth rate threshold in size homeostasis may not be as obvious a model as a size threshold; but there are several potential biochemical targets that could directly reflect the growth rate, and there are no known mechanisms in mammalian cells by which size itself could be sensed.

METHODS

Methods and any associated references are available in the online version of the paper.

Note: Supplementary information is available in the online version of the paper.

ACKNOWLEDGMENTS

We thank A. Miyawaki (RIKEN) for the *mKO2-hCdt1* and *mAG-hGem* constructs, M. Stevens (MIT), M. Ginzberg and R. Kafri (Harvard Medical School) for valuable discussions and M. Chung (Harvard Medical School) for assistance with generating the FUCCI-labeled L1210 cells. S.R.M. acknowledges support from US National Cancer Institute contracts Physical Sciences Oncology Center U54CA143874 and R21 CA137695 as well as from the National Institutes of General Medical Sciences (NIGMS) EUREKA R01GM085457. M.W.K. acknowledges support from the NIGMS. S.S. acknowledges support from the Kwanjeong Educational Foundation, South Korea, through a graduate fellowship. Y.W. acknowledges support from a National Science Foundation Graduate Research Fellowship, and A.T. acknowledges support from The Marie Curie International Reintegration Grant PIRG-GA-2010-277062 and the Israeli Centers of Research Excellence (I-CORE) program (Center no. 41/11).

AUTHOR CONTRIBUTIONS

S.S. and Y.W. developed methods for multigeneration cell growth measurements. A.T. transformed the L1210 cell line with FUCCI. S.S., A.T., P.J., M.W.K. and S.R.M. designed the experiments and analyzed the data. S.S. developed an optical system for simultaneous fluorescence measurement and performed the experiments. J.K. assisted with the data acquisition and cell culture. S.S., A.T., Y.W., P.J., M.W.K. and S.R.M. wrote the manuscript.

COMPETING FINANCIAL INTERESTS

The authors declare competing financial interests: details are available in the online version of the paper.

Published online at http://www.nature.com/doifinder/10.1038/nmeth.2133. Reprints and permissions information is available online at http://www.nature.com/reprints/index.html.

1. Mitchison, J.M. *Int. Rev. Cytol.* **226**, 165–258 (2003).
2. Jorgensen, P. & Tyers, M. *Curr. Biol.* **14**, R1014–R1027 (2004).
3. Conlon, I. & Raff, M. *Cell* **96**, 235–244 (1999).
4. Conlon, I. & Raff, M. *J. Biol.* **2**, 7 (2003).
5. Cooper, S. *BMC Cell Biol.* **5**, 35 (2004).
6. Conlon, I.J., Dunn, G.A., Mudge, A.W. & Raff, M.C. *Nat. Cell Biol.* **3**, 918–921 (2001).
7. Sveiczer, A., Novak, B. & Mitchison, J.M. *Theor. Biol. Med. Model.* **1**, 12 (2004).
8. Di Talia, S., Skotheim, J.M., Bean, J.M., Siggia, E.D. & Cross, F.R. *Nature* **448**, 947–951 (2007).
9. Davies, H.G. & Wilkins, M.H.F. *Nature* **169**, 541 (1952).
10. Burg, T.P. *et al. Nature* **446**, 1066–1069 (2007).
11. Godin, M. *et al. Nat. Methods* **7**, 387–390 (2010).
12. Sakaue-Sawano, A. *et al. Cell* **132**, 487–498 (2008).
13. Tzur, A., Kafri, R., LeBleu, V.S., Lahav, G. & Kirschner, M.W. *Science* **325**, 167–171 (2009).
14. Nurse, P. & Thuriaux, P. *Exp. Cell Res.* **107**, 365–375 (1977).
15. Nurse, P. *Nature* **286**, 9–10 (1980).

ONLINE METHODS

Suspended microchannel resonator (SMR). As described in ref. 16, cells suspended in solution flow through the SMR, and the resulting frequency shift depends on the mass and position of the particles. When a cell passes through the SMR, this measurement yields a peak whose height is directly proportional to the cell's buoyant mass. SMR devices are fabricated by first creating buried channels in silicon-on-insulator wafers; after, wafer thinning and dry etching are used to form suspended microchannels with 2- to 3-μm-thick walls and a 15-μm fluid layer. Two hundred devices are fabricated and vacuum-packaged on a 6-inch wafer, with yields exceeding 80%. A getter layer prevents slow degradation of the on-chip vacuum due to outgassing. Integrated under each cantilever is an electrostatic drive electrode, and the cantilever vibration is detected by the optical lever. A gain-controlled oscillator circuit is used to continuously track the resonance frequency of the SMR during the growth measurement.

Single-cell growth measurements. To achieve long-term growth measurements of single cells, an approach shown schematically in **Supplementary Figure 11** was devised to culture the cell within the two bypass reservoirs adjacent to the SMR. Computer-controlled pressure regulators with pressurized glass sample vials on vertical translational stages are used to precisely control fluid flow within the SMR chip. Every 30–60 s, feedback between the mass signal and pressure regulators causes the cell to transit from one bypass to the other within a period of approximately 1 s. This process is fully automated, and the specific sequence of steps used to capture and maintain the cell within the device is outlined in the caption of **Supplementary Figure 11**. Because the bypass reservoirs are optically transparent, the cell can be observed by a modular microscope (**Supplementary Video 1**). Upon division, both cells initially flow back and forth between the bypass channels. However, the feedback randomly selects the mass signal from one of the cells. As a result, the other cell slowly drifts away from the one in feedback and is eventually swept away in the bypass channels. To increase measurement precision, hydrodynamic focusing was used to minimize position-dependent error within the SMR (**Supplementary Fig. 2**).

L1210 culture and FUCCI expression. L1210 murine lymphoblasts (ATCC-CCL219) were adapted to Leibovitz's L-15 CO_2-independent medium (Invitrogen) and maintained in medium supplemented with 10% FBS (Invitrogen), 1 g/L D-(+)-glucose solution (Sigma-Aldrich) and 1% 100× penicillin-streptomycin solution (Gemini). For growth measurements in medium with limited isoleucine, L-15 medium without any isoleucine was supplemented with 10% FBS. The FUCCI constructs *mKO2* (monomeric Kusabira-Orange2)-*hCdt1* and *mAG* (monomeric Azami-Green)-*hGem*[17] were cloned into lentiviral vectors carrying the neomycin or blasticidin resistance genes, respectively. We generated virus particles by transfecting 293T cells and performing standard virus purification. L1210 cells were first infected (using Polybrene, 8 μg/ml) with *mAG-hGem*–carrying viruses. After selection (using 3 μg/ml blasticidin), cells were infected again with the *mKO2-hCdt1* viral particle and selected using 400 μg/ml of Geneticin to form the FUCCI L1210 line. Cells used in this study originated from a single cell.

Fluorescence measurement. A modular microscope (Nikon) was mounted on top of the SMR, and a 50× objective lens (Nikon-CFI Plan BD ELWD N.A. 0.55, W.D 9.8 mm) was used to collect the fluorescent signal into two separate photomultiplier tubes (H5784-02) (**Supplementary Figs. 12** and **13**). To measure red and green fluorescence simultaneously, wide-band metal halide illumination (Lumen-200pro) was used with a dual-cavity dichroic mirror (Chroma-59004) and single-cavity emission filters (red-ET585/40m, green-HQ520/20m; both Chroma). Illumination was shuttered by the light source, and two field stops were used to confine the area of illumination and imaging to minimize the background noise. Fluorescent signals were measured at the collimated plane.

pH stability for FL5.12 culture. RPMI (Invitrogen) cell growth media used for FL5.12 cells requires 5% CO_2 for bicarbonate buffering. To achieve this, the medium vials were pressurized with 5% CO_2 gas (Airgas), which stabilized the pH of medium in the vial. However, because of the CO_2 leakage in the tubing and the gasket, dissolved CO_2 was lost from the medium on the way to the chip and limited cell growth in the bypass channels. PEEK tubing (IDEX), which has minimum gas permeability, was used to reduce CO_2 leakage. Nevertheless, CO_2 leakage still occurred at the tubing–to–chip gasket interface. As a result, on-chip pH monitoring was required to determine the optimal flow conditions and device geometry for maintaining a stable pH. This was accomplished by using the fluorescent indicator BCECF (2′,7′-bis-(2-carboxyethyl)-5-(and-6)-carboxyfluorescein), which is often used for monitoring intracellular pH. The pH sensitivity of BCECF in the SMR optical system was calibrated by using a plate reader (Tecan). Real-time monitoring in the bypass reservoir revealed that the pH would increase within 1–2 h if the medium was not replenished with sufficient frequency (**Supplementary Fig. 14**). Because the medium replenishment rate is governed by the cell transit frequency (typically 1–2 times per minute), achieving stable pH came at the cost of exposing the cell to detrimentally high levels of shear. To overcome this, the SMR chip was designed with enlarged bypass reservoirs (cross-sectional dimensions were increased by twofold to 1,400 $\mu m^2 \times 2{,}800\ \mu m^2$), which allowed the replenishment rate to be increased by fivefold for the same transit frequency. As a result, a stable pH was observed for more than 15 h when the cell transited the SMR as infrequently as once every 100 s.

Data processing. To calculate the rate at which a cell accumulates biomass (growth rate) from measurements of buoyant mass versus time, the raw data (sampled every 30 s) were smoothed by a 30-min moving average window, and the time derivative was taken at each point. The buoyant mass and growth rate measurement errors were determined as the s.d. of the buoyant mass and growth rate measurements from either beads or fixed cells over acquisition periods greater than 12 h. Three steps were used to find the location of the growth rate transition. (i) A second-order polynomial was fit to the initial buoyant mass versus time trajectory with progressively longer time windows. (ii) The duration of the window for when the fitting error increased above a defined threshold was determined. (iii) The size and growth rate at the end of the time window was then used in a bilinear fit as an initial value of the growth rate transition point. The bilinear fit of the growth rate over buoyant mass provided four parameters: growth rate acceleration before and after the transition, mass and growth rate at the transition point.

16. Burg, T.P. *et al. Nature* **446**, 1066–1069 (2007).
17. Sakaue-Sawano, A. *et al. Cell* **132**, 487–498 (2008).

doi:10.1038/nmeth.2133

Direct observation of mammalian cell growth and size regulation

Sungmin Son, Amit Tzur, Yaochung Weng, Paul Jorgensen, Jisoo Kim, Marc W. Kirschner and Scott R. Manalis

Nature Methods: doi:10.1038/nmeth.2133

Supplementary Figure 1 | L1210 interdivision time for single cell and bulk cultures

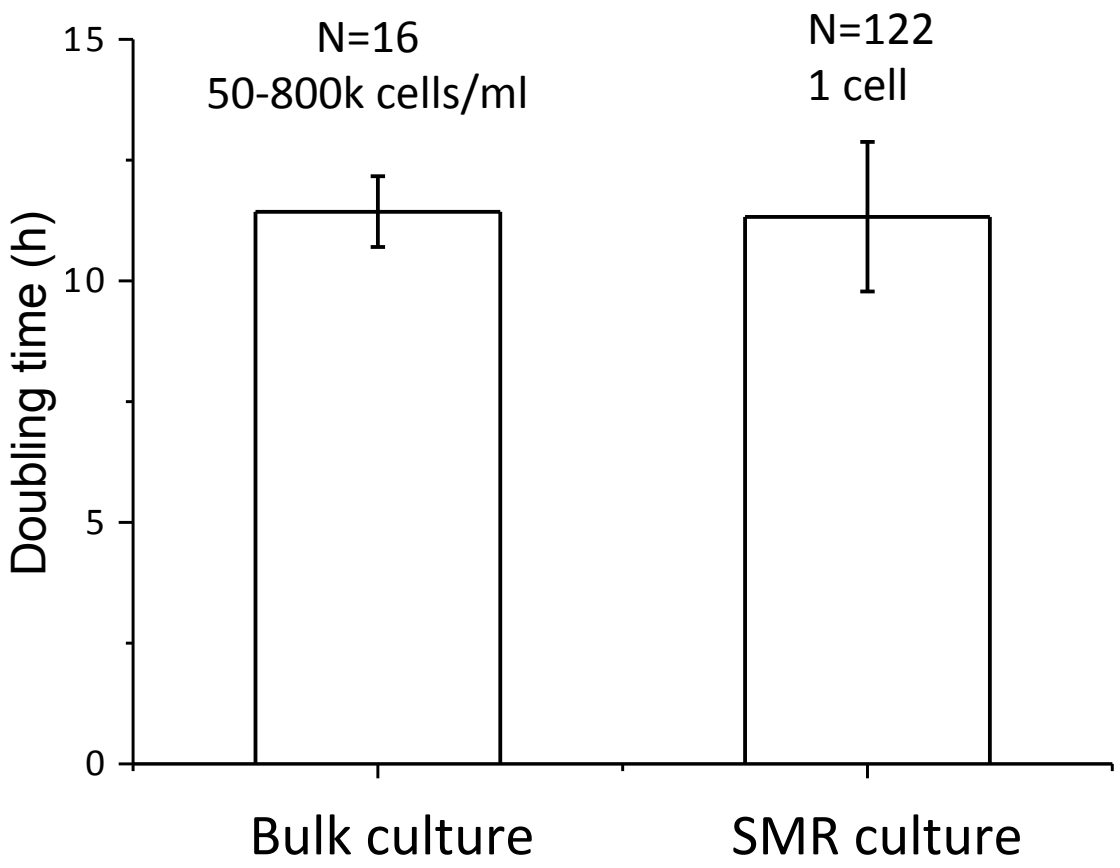

The doubling time of bulk culture as measured by the Coulter Counter was 11.4 ± 0.7 (s.d.) hours which is in agreement with the interdivision time of 11.3 ± 1.5 (s.d.) hours for single cells grown in the SMR chip.

Nature Methods: doi:10.1038/nmeth.2133

Supplementary Figure 2 | Hydrodynamic focusing constrains the flow path of a cell that transits the SMR

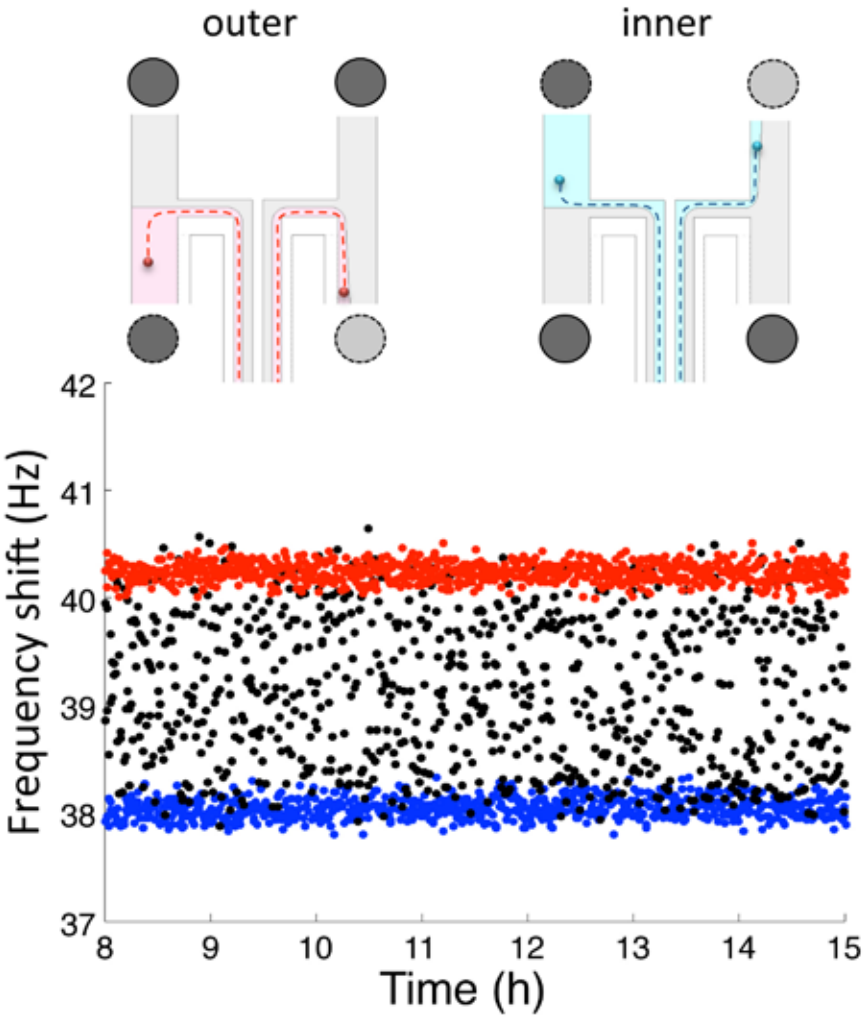

The cartoon shows the pressure configurations in the four ports: high pressure (dark grey) and low pressure (light grey). Solid black lines indicate a fixed pressure and dashed black lines indicate an alternating pressure. If a pressure gradient exists along the bypass channel, then particles that enter the SMR will travel through it with a highly variable flow path. This is evident when the resonant frequency shift from a 12 µm polystyrene bead is repetitively measured (black points on plot). By balancing the pressure along the bypass, flow enters the SMR from the top and bottom sides and the particle's path is focused. The dashed red line in the cartoon indicates focusing through the outer flow path (red points on plot) and the dashed blue line indicates focusing through the inner flow path (blue points on plot).

Nature Methods: doi:10.1038/nmeth.2133

Supplementary Figure 3 | Growth rate acceleration ratio at the G1-S transition

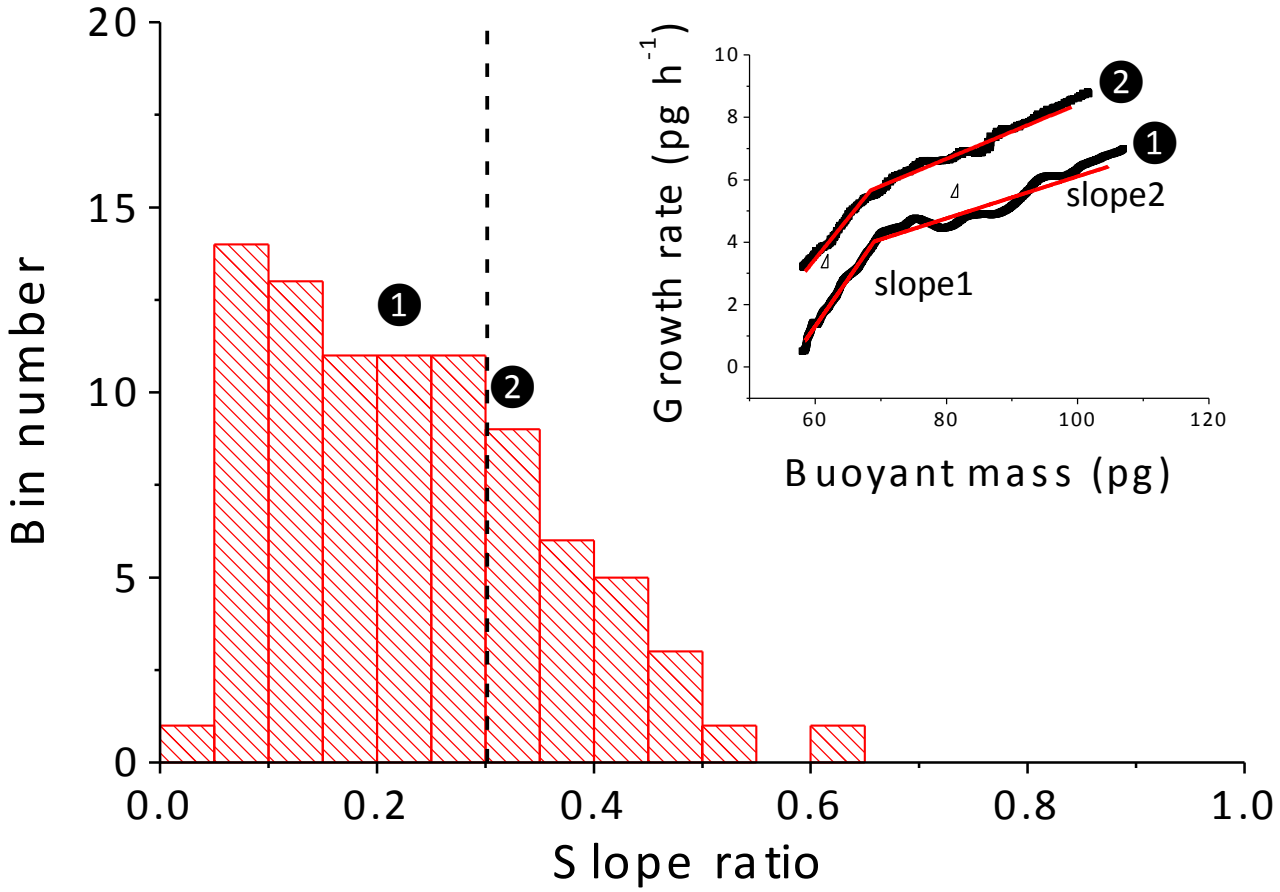

Histogram shows the distribution of the slope ratio, which is defined by the growth rate acceleration just after the G1/S transition divided by acceleration just before the G1-S transition. The transition point was determined by a bilinear curve fit (Online Methods). There were 61 cells (out of 122) that exhibited slope ratios below 0.3 and 25 cells with ratios between 0.3 to 0.7. Inset shows two representative trajectories: ❶ slope ratio of 0.22, ❷ slope ratio of 0.34.

Nature Methods: doi:10.1038/nmeth.2133

Supplementary Figure 4 | Growth rate trajectories of cell lineages

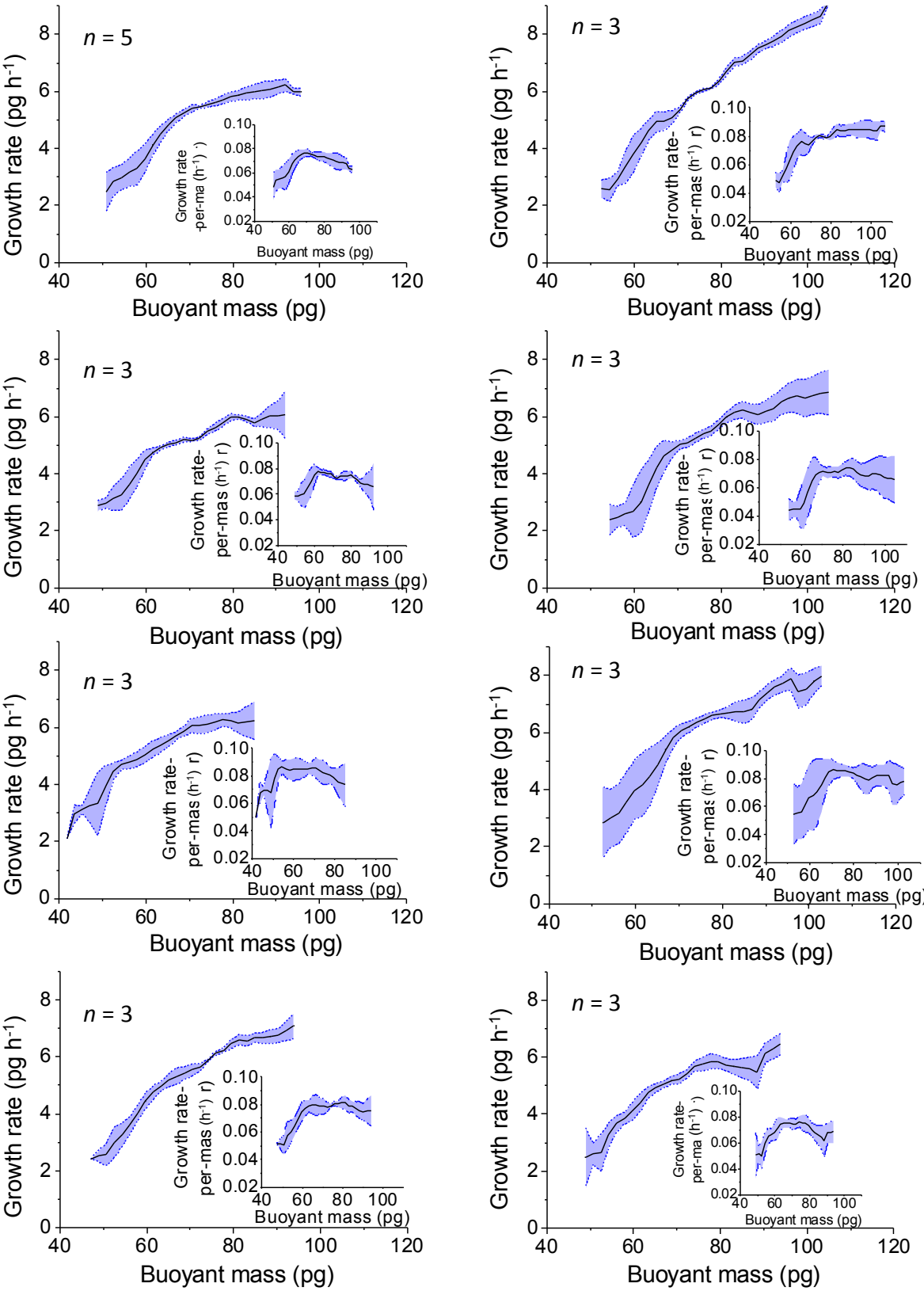

The black lines show the mean growth trajectory from all cells in a particular lineage and the blue shaded region is defined by three times the coefficient of variance. Inset: The mean (black line) and standard deviation (blue area) of the growth rate-per-mass versus mass for the lineage.

Nature Methods: doi:10.1038/nmeth.2133

Supplementary Figure 5 | G1 duration versus early G1 growth rate in media with limited isoleucine

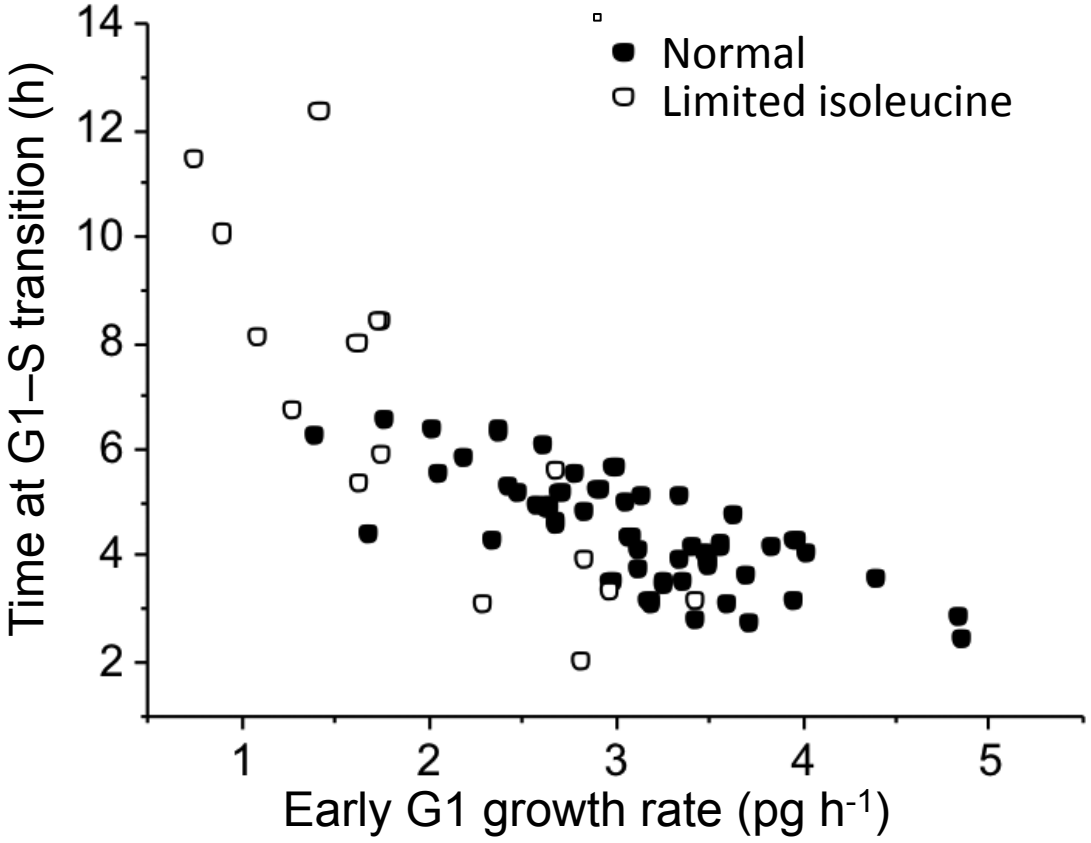

A negative correlation becomes more apparent when cells are grown under limited isoleucine conditions. Early G1 growth rate is determined by averaging the mass accumulation rate between the first and third hour following cell division. Normal: n = 49, Pearson's correlation coefficient = –0.75; Limited isoleucine: n = 16, Pearson's correlation coefficient = –0.83.

Nature Methods: doi:10.1038/nmeth.2133

Supplementary Figure 6 | Interdivision and G1 time versus newborn cell size

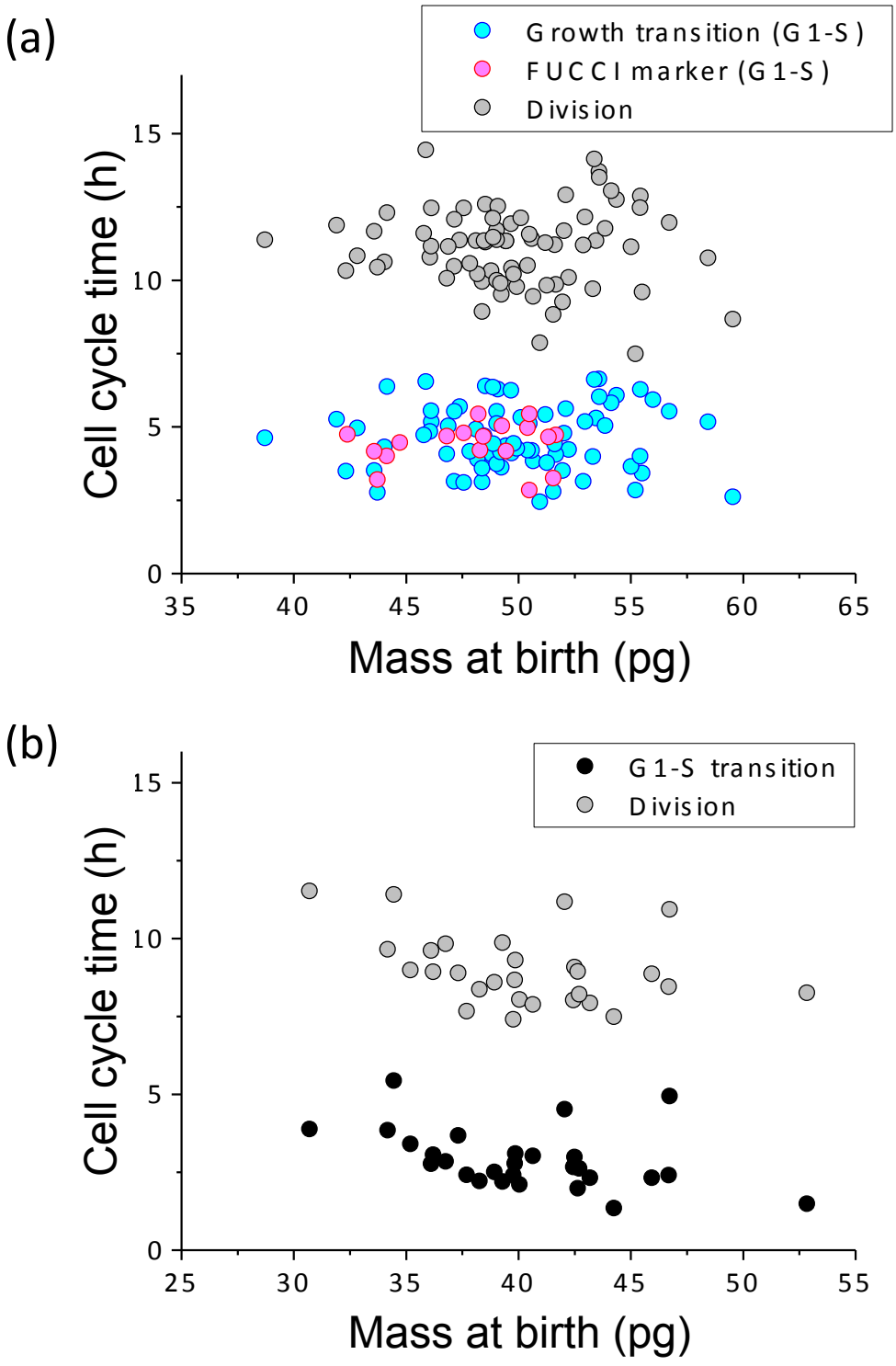

(**a**) L1210 mouse lymphoblast cells. Blue and red circles: Time at G1/S transition versus mass at birth (blue *n* = 77, Pearson's correlation coefficient = 0.03, red *n* = 18, Pearson's correlation coefficient = 0.10). Grey circles: time at division versus mass at birth (*n* = 122, Pearson's correlation coefficient = 0.08). (**b**) FL5.12 pro-B-cell lymphoid cells**.** Black circles: time at G1/S transition versus mass at birth (*n* = 28, Pearson's correlation coefficient = –0.42), Grey circles: time at division versus mass at birth (*n* = 28, Pearson's correlation coefficient = –0.36).

Nature Methods: doi:10.1038/nmeth.2133

Supplementary Figure 7 | Lineage growth trajectories for L1210 and FL5.12 cells

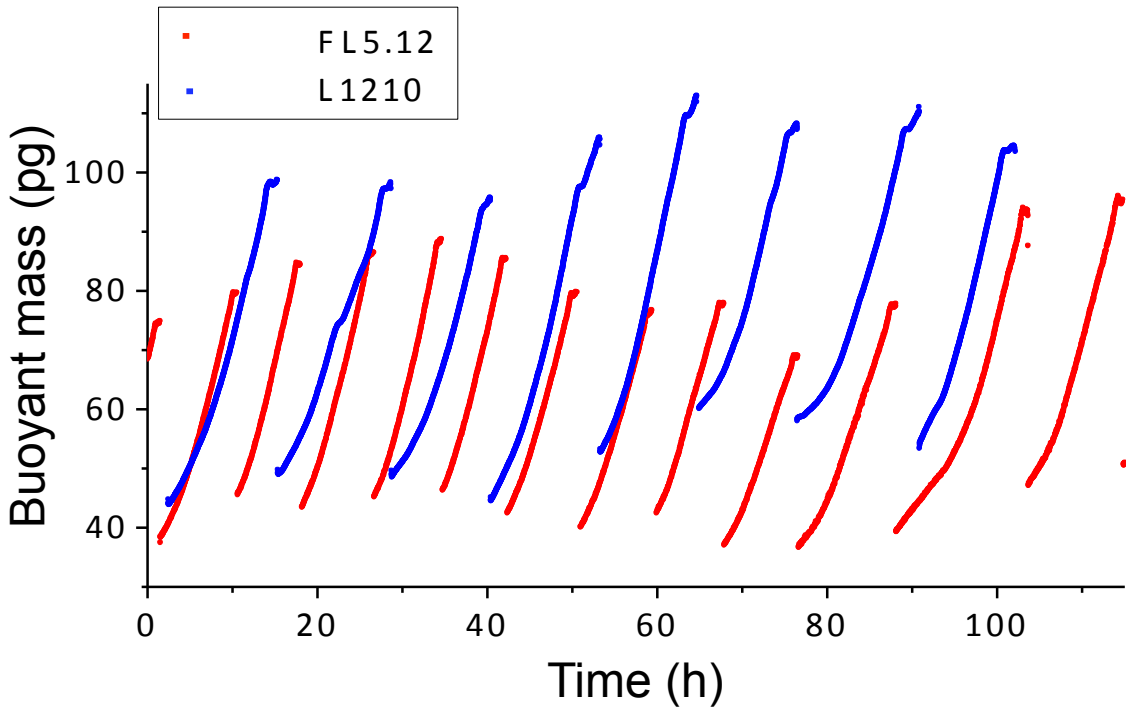

Nature Methods: doi:10.1038/nmeth.2133

Supplementary Figure 8 | Growth of L1210 cells in media with limited isoleucine

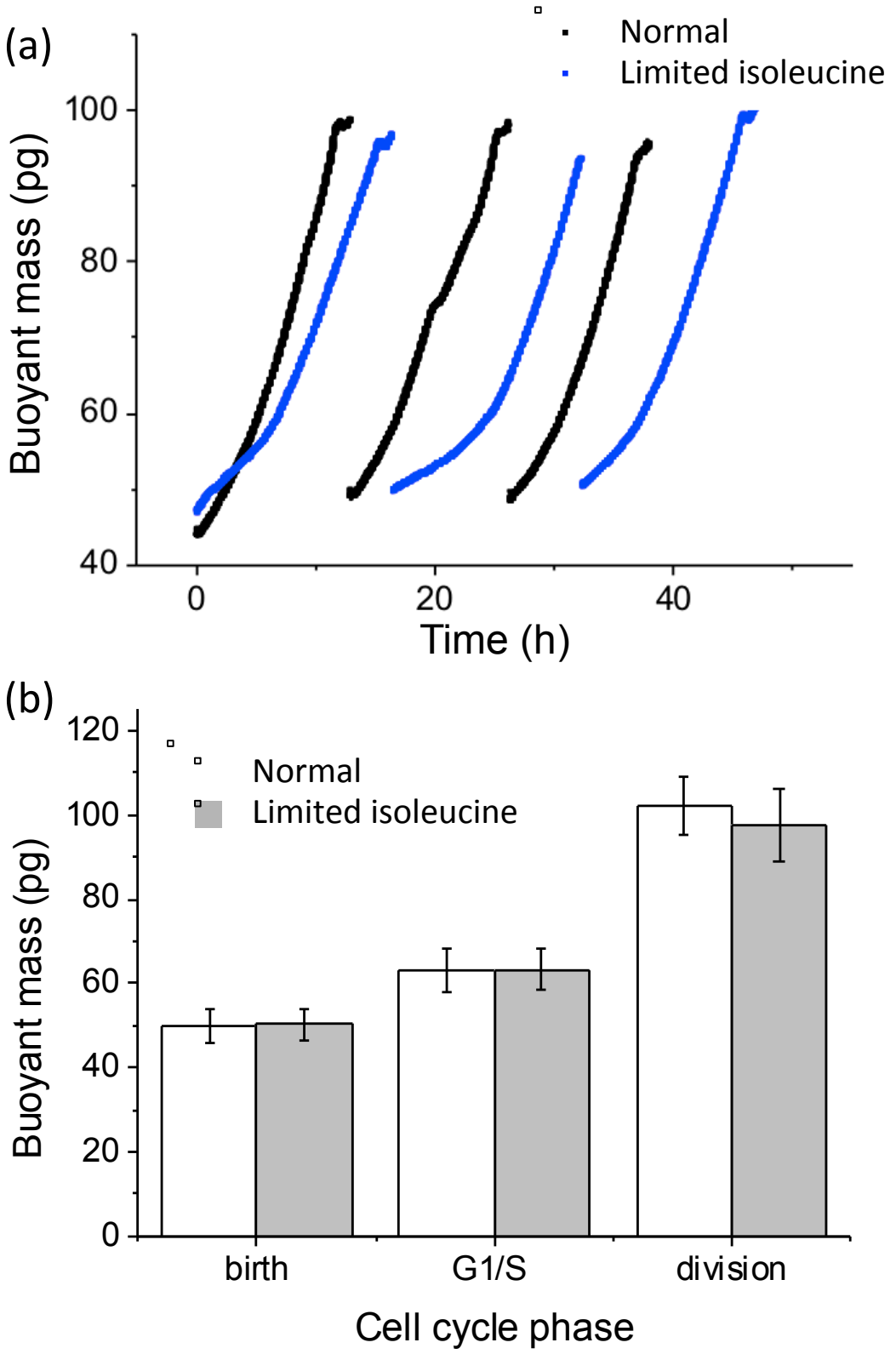

(**a**) Representative growth curves of lineages grown in different environments. The black line indicates cells grown in normal media and the blue line under limiting amount of Isoleucine. (**b**) The columns show the mean size of cells at birth, G1–S transition and division. *n* = 77 for normal; *n* = 17 for limited isoleucine.

Nature Methods: doi:10.1038/nmeth.2133

Supplementary Figure 9 | Size distributions of steady-state cell cultures in normal and media with limited isoleucine

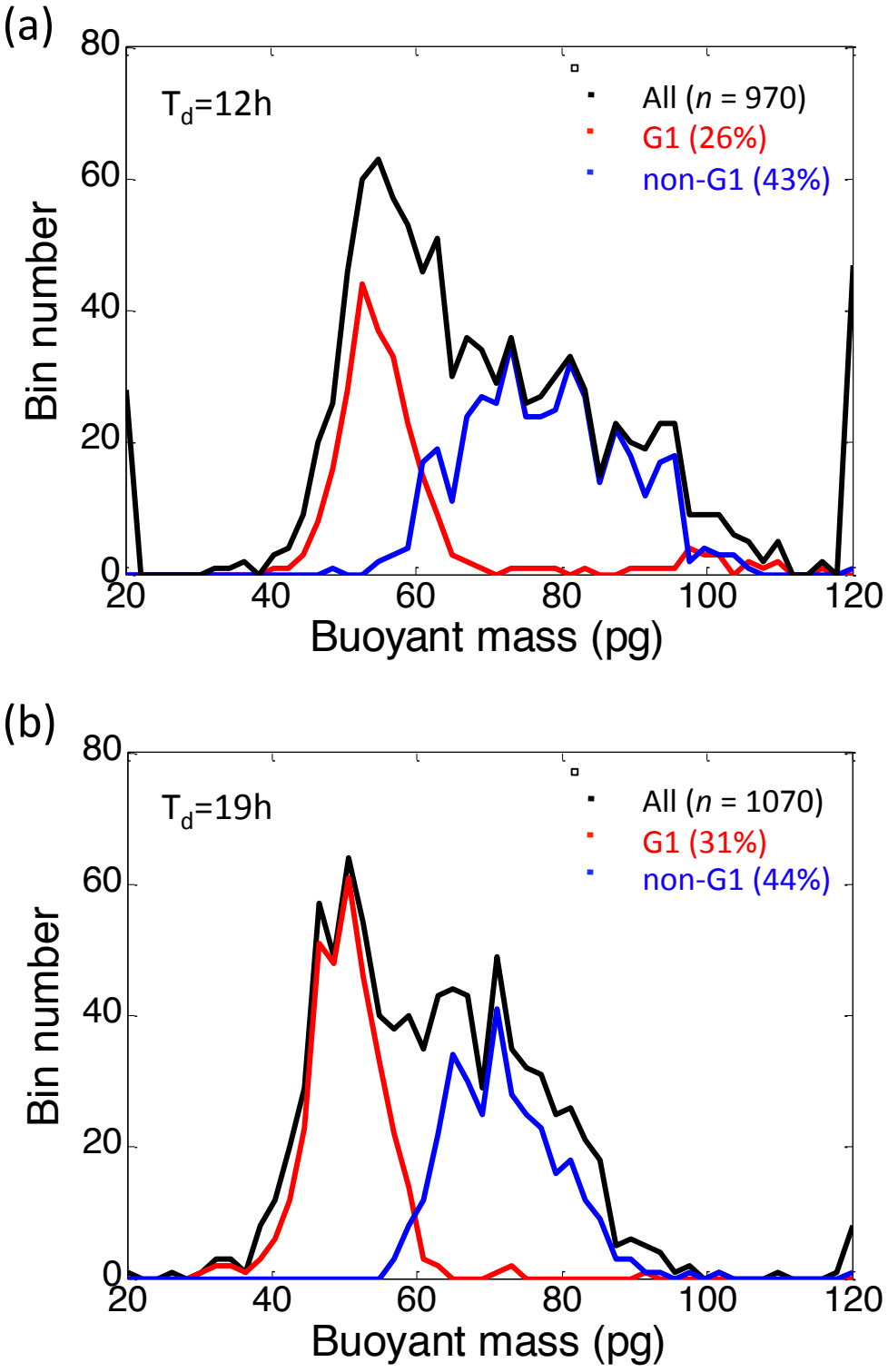

G1 (red) or post G1 (blue) cells are measured from a steady-state cell culture. Black line indicates entire population. (**a**) normal media (12 h doubling time), (**b**) limited isoleucine media (19 h doubling time).

Nature Methods: doi:10.1038/nmeth.2133

Supplementary Figure 10 | Lineage trajectories for cells grown in normal and media with limited isoleucine

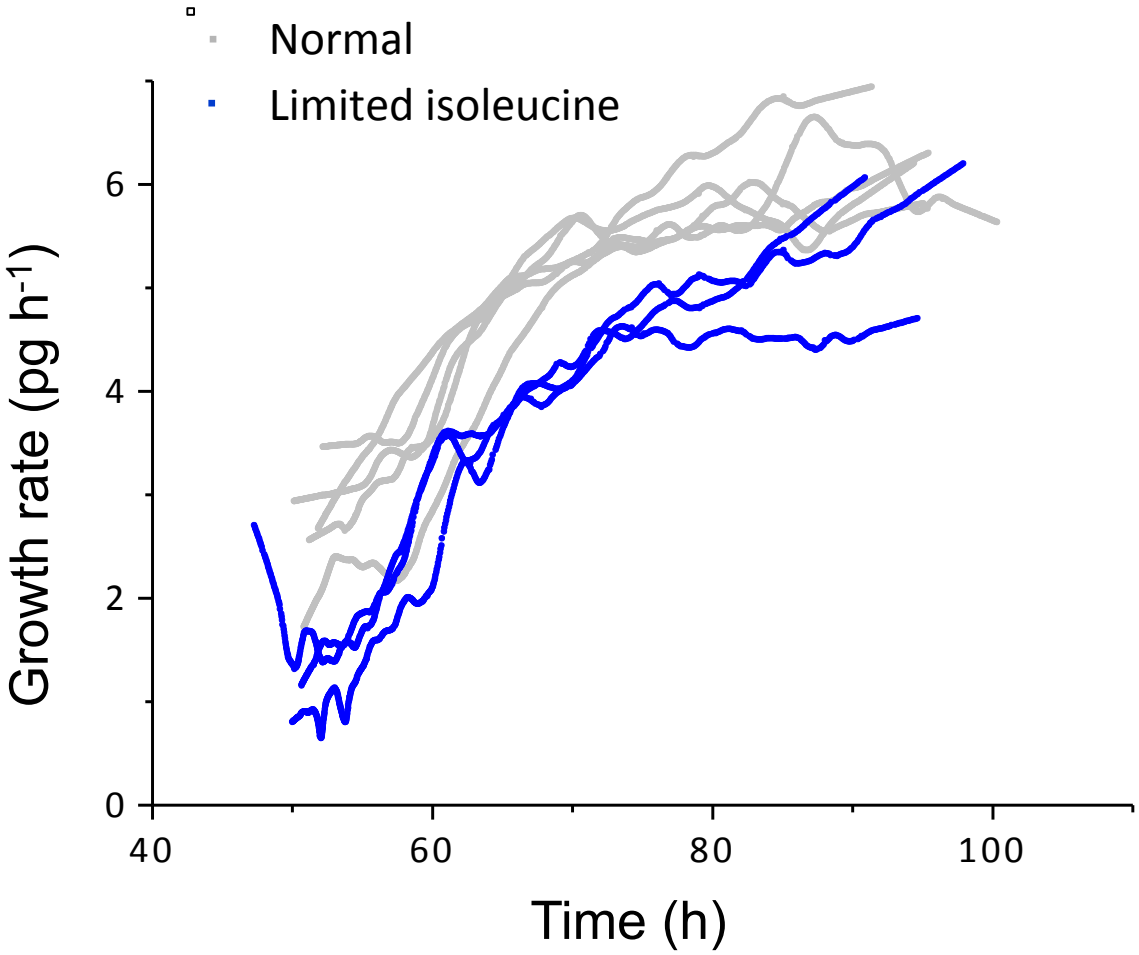

Nature Methods: doi:10.1038/nmeth.2133

Supplementary Figure 11 | Single cell loading in SMR for long-term growth measurement

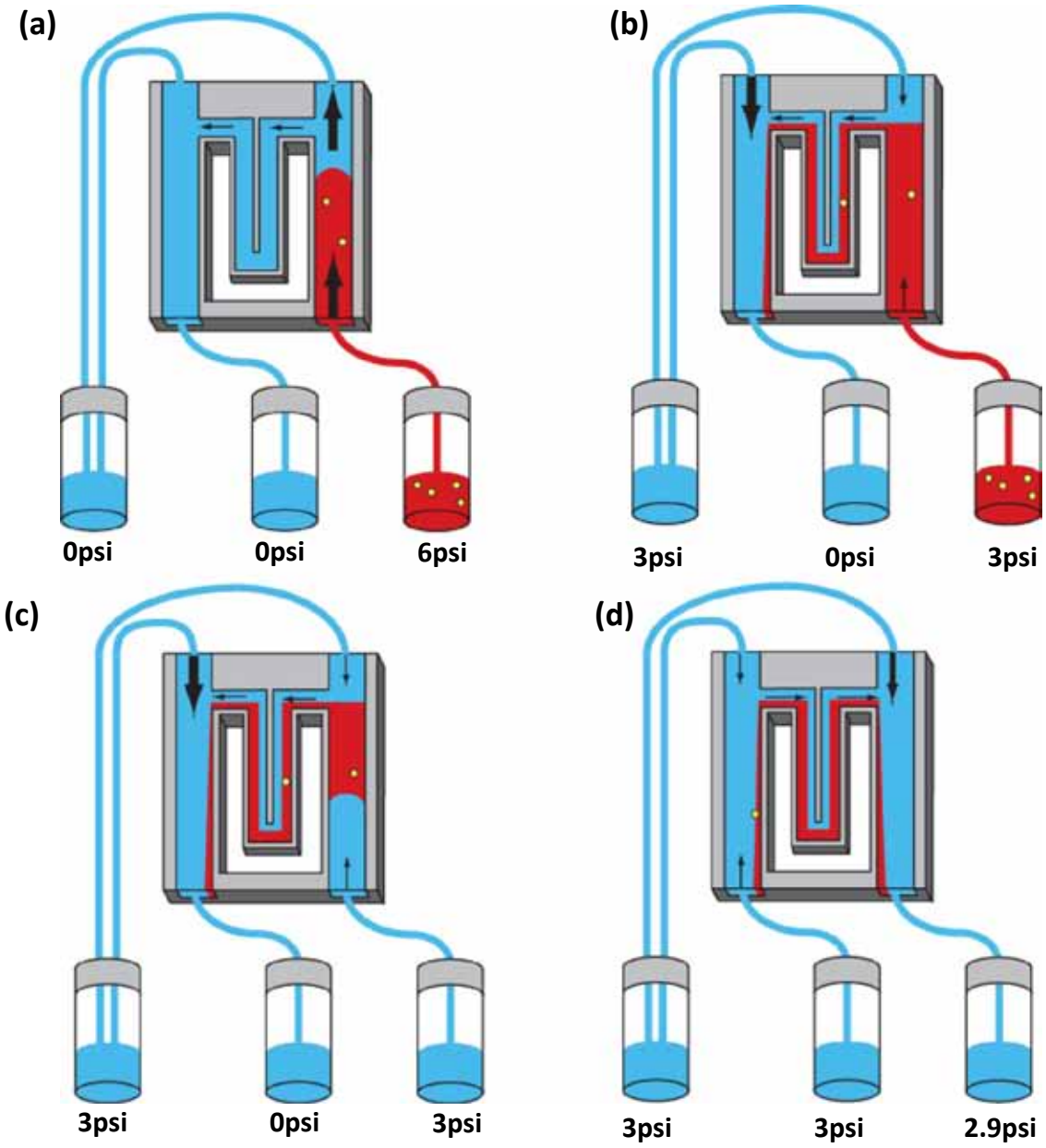

(**a**) One upstream and two downstream vials are pressurized by independent pressure regulators. The system is primed with media (blue) before a cell is loaded. During cell loading, only the downstream vial on the right is pressurized (6 psi) and the sample plug (red) flows into the chip. The flow rate is qualitatively shown with the thick (high) and thin (low) arrows. (**b**) As the sample plug moves toward the SMR, an equal pressure (3 psi) is applied to both the upstream and downstream vials. By balancing the pressure applied across the bypass, fluid from both the upstream and downstream directions enter the SMR. As a result, the flow path of the cell is confined to either the inner or outer region of the channel, which minimizes the position dependent error (see Supplemental Figure 2). (**c**) After the sample has been completely loaded, all pressure sources are turned off and the sample vial is exchanged to media. The downstream vial is then pressurized again to keep the cell in transit. (**d**) As soon as a cell of a desirable size transits through the SMR, the flow direction is reversed and the flow rate is reduced by elevating the downstream pressure to 2.9 psi. The sample plug on the right bypass channel is rinsed away by flow from the upstream direction. The liquid level in all three vials is matched in order to remove any leakage flow induced by variations in hydrostatic pressure.

Supplementary Figure 12 | SMR optical system for single cell fluorescence measurement

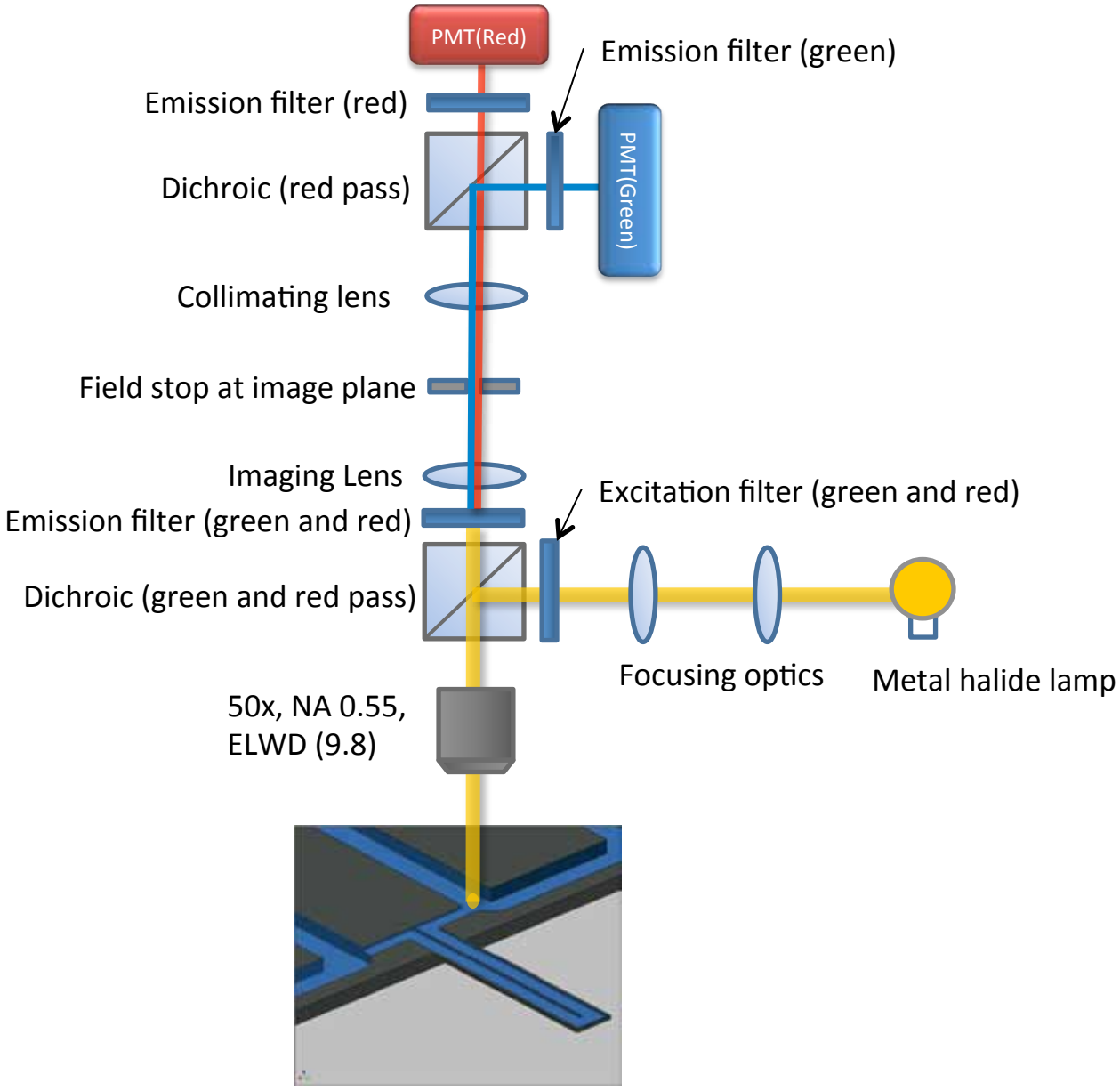

Nature Methods: doi:10.1038/nmeth.2133

Supplementary Figure 13 | Sensitivity and precision of the SMR optical system

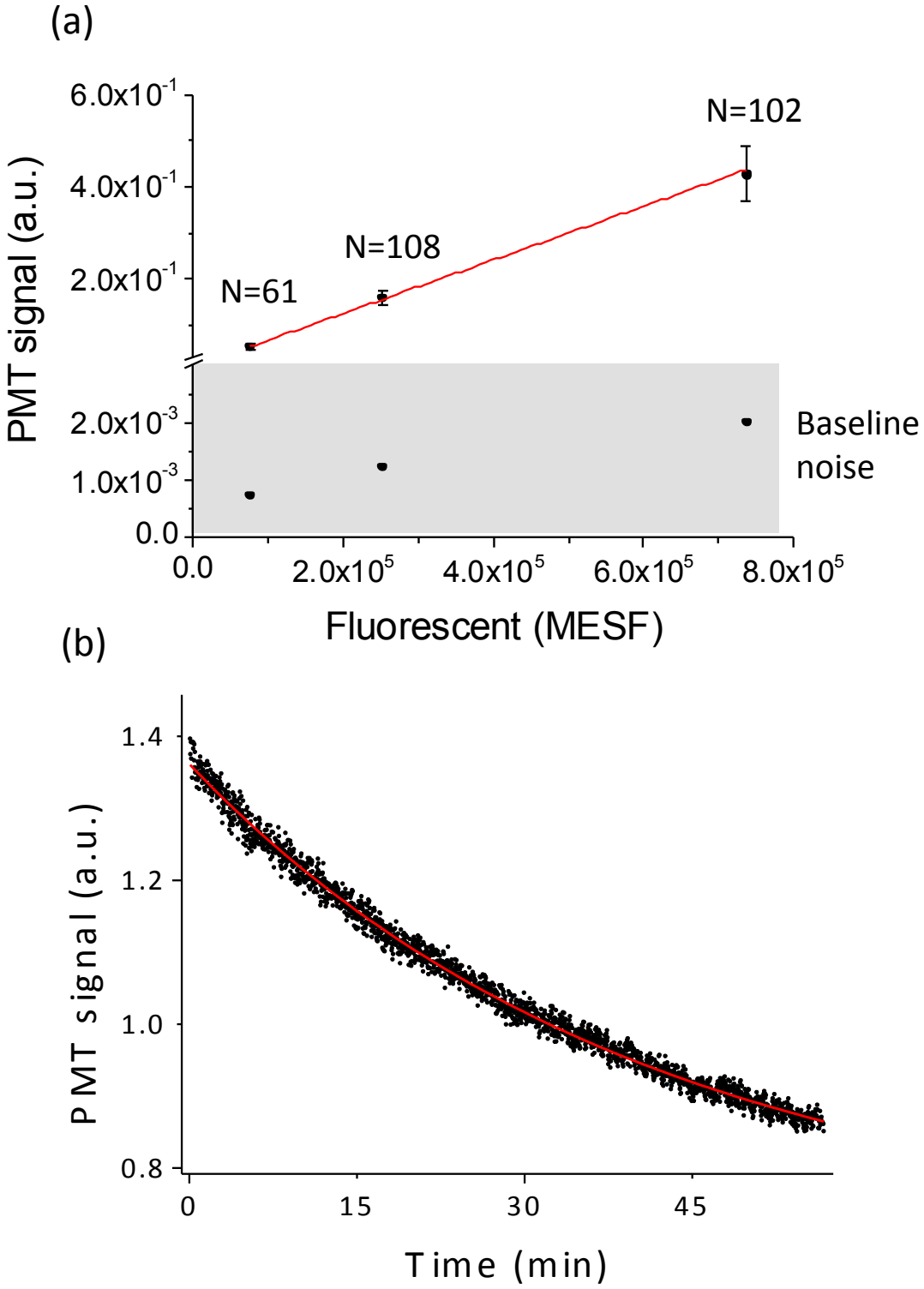

(**a**) Mean and standard deviation of the fluorescent signals from three different populations of MESF standard beads. Linear fit (red, $r^2 = 0.998$) shows the sensitivity of 5.8×10^{-7}/MESF. The corresponding baseline noise for three different signals are shown at the bottom of the plot (one sigma, acquired at 10Hz bandwidth). The signal-to-noise ratio is 70, 130, and 210, for the *n* = 61, 108, and 102 measurements, respectively. (**b**) The fluorescent signal of the same bead is repeatedly measured every 3 seconds for ~1hr. The signal exponentially decays due to photo-bleaching. The RMSE is 1%.

Nature Methods: doi:10.1038/nmeth.2133

Supplementary Figure 14 | pH stability in the bypass reservoir

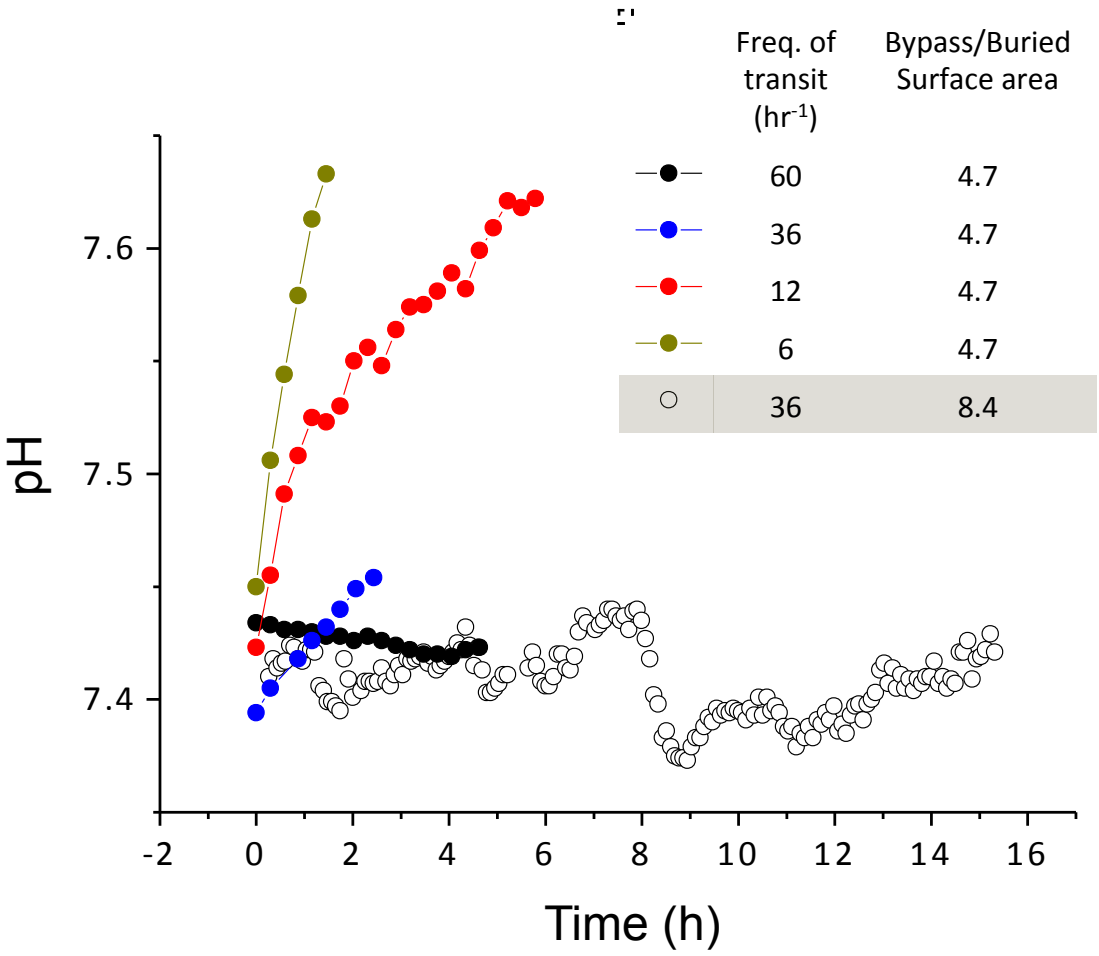

The pH in the bypass reservoir was measured over time for four cell transit conditions and two SMR chip designs (see Table). Transit conditions were determined by how frequently the cell transited through the SMR, which together with the bypass-to-buried surface area ratio, determined the media replenishment rate in the chip. pH in the chip slowly increased when the replenishment rate was too low due to the local leakage of CO_2 that occurs in the tubing-to-chip gasket interface. For the design with the low bypass-to-buried-surface-area ratio, it was necessary to transit the cell every minute in order to maintain constant pH (black filled circles). However, for FL5.12 cells, this level of shear stress was detrimental. By using a SMR chip with a larger bypass-to-buried-surface-area ratio, the pH was stably maintained over extended periods of time with a low transit frequency (black open circles).

Nature Methods: doi:10.1038/nmeth.2133